


## Fragmentation dynamics of $\text{CO}_2^{4+}$ : Contributions of different electronic states

Sumit Srivastav , Arnab Sen , Deepak Sharma , and Bhas Bapat\*

*Indian Institute of Science Education and Research Pune, Homi Bhabha Road, Pune 411008, India*

 (Received 18 December 2020; revised 23 February 2021; accepted 1 March 2021; published 16 March 2021)

Fragmentation of  $\text{CO}_2^{4+}$ , created by the impact of slow, highly charged ions (96 keV  $\text{Ar}^{q+}$ ;  $8 \leq q \leq 14$ ) on  $\text{CO}_2$ , has been studied by recoil ion momentum spectrometry.  $\text{CO}_2^{4+}$  was found to dissociate into three ionic fragments through two channels:  $\text{CO}_2^{4+} \rightarrow \text{O}^+ + \text{C}^{2+} + \text{O}^+$  [the (1,2,1) channel] and  $\text{CO}_2^{4+} \rightarrow \text{O}^{2+} + \text{C}^+ + \text{O}^+$  [the (2,1,1) channel]. The kinetic energy of each fragment ion and the total kinetic energy release (KER) distributions for these channels were derived. *Ab initio* quantum chemical calculations at the multiconfiguration self-consistent-field configuration-interaction level of theory were carried out to obtain the potential energy curves of  $\text{CO}_2^{4+}$ , from which the expected KER values were derived. A comparison of the experimental KER distributions with the expected KER values for different excited states enabled the estimation of the relative probabilities of accessing different electronic states of  $\text{CO}_2^{4+}$ . These probabilities were found to depend on the projectile charge  $q$ . The fragmentation was visualized using the Dalitz plots, which revealed that the (1,2,1) channel arises exclusively via concerted fragmentation, while the (2,1,1) channel also has a small contribution from sequential fragmentation.

DOI: [10.1103/PhysRevA.103.032821](https://doi.org/10.1103/PhysRevA.103.032821)

### I. INTRODUCTION

The dissociation dynamics of multiply ionized polyatomic molecules has been a topic of study in recent years [1–5]. With the rapid development of momentum imaging techniques [6,7], it is now possible to map the momentum vectors of all ionic fragments in coincidence. However, obtaining detailed kinematics of polyatomic molecular ions has been a challenge because of many-body involvement in the dissociation channels. Several experiments have been carried out addressing the question of whether the multiply ionized triatomic molecular ion of molecules such as  $\text{CO}_2$ ,  $\text{CS}_2$ ,  $\text{N}_2\text{O}$ , or  $\text{OCS}$  dissociate via a concerted process or sequential process [2,4,8,9]. In a concerted process, all bonds of the molecular ion break simultaneously and the atomic ions move apart due to their Coulomb repulsion. In the other extreme process of sequential or stepwise dissociation, the molecular ion first separates into two ionic fragments and, after some time when they hardly interact with each other, the second step of dissociation occurs.

$\text{CO}_2$  has been regarded as a prototype molecule for the study of three-body fragmentation dynamics and has captured a lot of attention. In this context,  $\text{CO}_2^{3+}$  is one of the most studied molecular cations of  $\text{CO}_2$ , created under the action of a variety of projectiles such as slow ( $v < 1$  a.u.) [2], intermediate velocity ( $v \approx 1$  a.u.) [10], and swift ( $v > 1$  a.u.) highly charged ions (HCIs) [11–14], electron impact [15,16], synchrotron radiation [17,18], or femtosecond laser pulses [19–22]. A large number of these investigations [2,10,15,22] were centered around the separation of different fragmentation pathways, i.e., concerted and sequential processes, and the corresponding kinetic energy release (KER) distributions. By analyzing the KER distributions of  $\text{CO}_2^{3+}$  fragmentation,

Neumann *et al.* [2] concluded that the total energy deposited into the system is the key parameter to control the fragmentation dynamics. Using *ab initio* calculations, Wang *et al.* could identify the participating electronic states of  $\text{CO}_2^{3+}$  in its three-body fragmentation [15].

However, studies of the three-body fragmentation dynamics of  $\text{CO}_2^{n+}$  ( $n \geq 4$ ) are rather scarce. In studies of the fragmentation dynamics of  $\text{CO}_2^{n+}$  ( $3 \leq n \leq 6$ ) under the action of an intense laser field, a dependence of the KER distribution on the pulse width was observed [20,21]. Siegmann *et al.*, using swift HCIs,  $\text{Xe}^{18+}$  and  $\text{Xe}^{43+}$  at 5.9 MeV/u, explored KER distributions of different dissociation channels of  $\text{CO}_2^{n+}$  ( $3 \leq n \leq 6$ ) [11]. Khan *et al.*, using 1 MeV  $\text{Ar}^{8+}$  ions, explored concerted and sequential processes in the fragmentation of  $\text{CO}_2^{4+}$  and  $\text{CO}_2^{5+}$  [10]. Wang *et al.*, using 500 eV electrons, studied two fragmentation channels:  $\text{CO}_2^{4+} \rightarrow \text{O}^+ + \text{C}^{2+} + \text{O}^+$  [the (1,2,1) channel] and  $\text{CO}_2^{4+} \rightarrow \text{O}^{2+} + \text{C}^+ + \text{O}^+$  [the (2,1,1) channel] [23]. Significant differences in peak positions and the shape of the KER distributions of these two channels were observed. The differences were attributed to different states of  $\text{CO}_2^{4+}$  being accessed.

The charge of the projectile is an important parameter that decides the strength of the perturbation, and hence experiments on the creation and fragmentation of molecular ions under a range of projectile charges open up the possibility of preferentially populating different excited states. In the slow collisions with HCI, various electronic states of  $\text{CO}_2$  may get populated by different ionization mechanisms such as direct ionization or, more probably, by electron capture from the target molecule. In the present study, we investigate the (1,2,1) and (2,1,1) dissociation channels of  $\text{CO}_2^{4+}$  created by the impact of slow HCIs ( $\text{Ar}^{q+}$ ;  $8 \leq q \leq 14$ ) at 96 keV ( $v \approx 0.31$  a.u.) on  $\text{CO}_2$ . We observe total KER distributions of both fragmentation channels. We calculate the potential energy curves (PECs) of  $\text{CO}_2^{4+}$  by performing *ab initio*

\*bhas.bapat@iiserpune.ac.in

quantum chemical calculation based on multiconfiguration self-consistent-field configuration interaction (MCSCF-CI) and, with the help of computed PECs, estimate the KER values. By fitting the experimental KER distributions to a sum of distributions based on the computed estimates, we identify the contributions of different excited states to the fragmentation. We present the relative probabilities of accessing different excited electronic states of  $\text{CO}_2^{4+}$  dissociating into the (1,2,1) and (2,1,1) channels and their variation with the projectile charge. In addition, the fragmentation mechanisms of both channels have also been visualized using the Dalitz plot method. This analysis reveals that a symmetric concerted process dominates the (1,2,1) channel, while the (2,1,1) channel arises mainly through an asymmetric concerted process with a weak signature of sequential fragmentation.

## II. EXPERIMENTAL DETAILS

The present experiment has been carried out at the electron beam ion source (EBIS) facility at IISER Pune [24]. The source is manufactured by Dreebit GmbH, Germany, operated at room temperature [25]. It can deliver ions of charge state up to  $\text{Ar}^{16+}$ . The whole system can be raised to 5–25 kV positive potential and allowing extraction of ions with energy up to 5–25 keV/ $q$ . The capability of the EBIS to deliver ions of all charge states within a range makes it a very convenient tool for a systematic study of projectile charge dependence of fragmentation dynamics. Fragments resulting from the collision were analyzed using a multihit capable ion momentum spectrometer. The details of the momentum spectrometer and experimental setup can be found elsewhere [26]. Briefly, an Ar-ion beam from EBIS overlaps with the effusive beam of the target gas molecule  $\text{CO}_2$  at the center of the collision chamber housing the recoil ion momentum spectrometer. The momentum spectrometer is a single-field time-of-flight (ToF) spectrometer combined with a two-dimensional position ( $x, y$ ) sensitive detector. The ion acceleration region is of length 110 mm followed by a field-free drift region of length 220 mm so as to satisfy the Wiley-McLaren space focusing condition [27]. The fragment ions are guided towards the detector by a uniform electric field of strength 60 V/cm. The direction of the field is taken to be the  $+z$  direction. The ion detector is an 80-mm-diameter microchannel plate with a delay-line anode. Ejected electrons are detected by a channeltron mounted on the opposite side. The ion time-of-flight measurement is triggered by coincidence with the ejected electrons. Ion time of flight ( $t$ ) and arrival positions ( $x, y$ ) are recorded in list-mode format. The recorded data are analyzed offline after completion of the experiment. The raw selection of three-body fragmentation events is by simple triple ion coincidence; further refinement is done by imposing the momentum conservation condition, ensuring that the ionic fragments arise from the dissociation of the same molecular ion [26]. The low ion beam current, of the order of 10–15 pA, and low gas pressure ( $2\text{--}5 \times 10^{-7}$  mbar) are maintained to keep accidental coincidences at a lower rate. The  $t, x, y$  information is mapped one to one to the momentum components  $p_z, p_x, p_y$  of the fragments. From this information, the kinetic energy of all ionic fragments is derived. Fragmentation of highly charged molecular ions such as  $\text{CO}_2^{4+}$  results in rather high kinetic

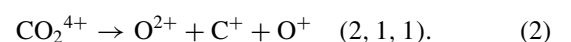
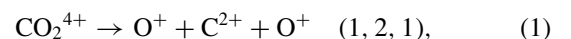
energy atomic ions, and efficient collection of these while also realizing adequate energy resolution is a challenge. In this experiment, an extraction field of 60 V/cm has been applied and the achieved resolution of the total kinetic energy is  $\approx 1.0$  eV. Based on the simulations, it was found that fragment ions with energies up to 8.5 eV/ $q$  are transported without loss to the detector, irrespective of their direction of emission from the interaction volume. Postcollision charge state analysis of the projectile, which can be useful for separating various ionization mechanisms such as direct and capture ionization, is not possible in the present experimental setup.

## III. COMPUTATION OF POTENTIAL ENERGY CURVES

Potential energy curves (PECs) of the several excited states of  $\text{CO}_2^{4+}$  leading to  $\text{O}^+ + \text{C}^{2+} + \text{O}^+$  and  $\text{O}^{2+} + \text{C}^+ + \text{O}^+$  dissociation have been calculated through *ab initio* calculations using the GAMESS [28] suite of programs. The multiconfiguration (MC) self-consistent-field (SCF) method [29] along with configuration interaction (CI) has been used to obtain the PECs of the excited states. The electronic configuration of the neutral  $\text{CO}_2$  ( $^1\Sigma^+$ ) is  $(1\sigma_u)^2(1\sigma_g)^2(2\sigma_g)^2(3\sigma_g)^2(2\sigma_u)^2(4\sigma_g)^2(3\sigma_u)^2(1\pi_u)^4(1\pi_g)^4$ . In the MCSCF-CI calculation, the inner five molecular orbitals are considered as a core orbital and the rest of the orbitals along with four virtual orbitals are taken as active orbitals with eight active electrons for the  $\text{CO}_2^{4+}$  ion. The density convergence criterion for this calculation has been set at  $10^{-6}$  to obtain well-converged virtual orbitals. For the (2,1,1) dissociation limit, the MCSCF calculation is carried out with point group symmetry  $C_1$ , where the two oxygen atoms are no longer equivalent to each other. However, for the (1,2,1) channel, the point group symmetry is taken to be  $D_{2h}$ , as it imposes two oxygen atoms to be identical. We have assumed symmetric stretch of the O–C–O bond from its equilibrium bond length of  $\approx 1.16$  Å up to  $\approx 10$  Å with a step size of 0.02 Å, and the energy of the excited states at each step is noted to get the entire PEC. In this case, three different basis sets, (i) split valence double zeta basis, (ii) Pople's triple split 6311-G basis set, and (iii) Dunning-type correlation consistent basis sets augmented with a set of diffuse function (aug-cc-pVTZ), are used to make sure that the calculated PECs are independent of the basis set. To validate our calculations, we have reproduced the PECs of neutral  $\text{CO}_2$  ( $^1\Sigma^+$ ) and excited states of  $\text{CO}_2^{3+}$ , which lead to the  $\text{O}^+ + \text{C}^+ + \text{O}^+$  dissociation. Our calculation shows a good match with previous results [15].

## IV. RESULTS AND DISCUSSION

Since the timescale for multiple ionization is approximately 10 fs [30,31] and the projectile-target interaction time in our experiment is subfemtoseconds, we can assume a vertical transition from the ground state of  $\text{CO}_2$  to its multiply ionized state. Three-body fragmentation channels of  $\text{CO}_2^{4+}$  observed in the experiment are



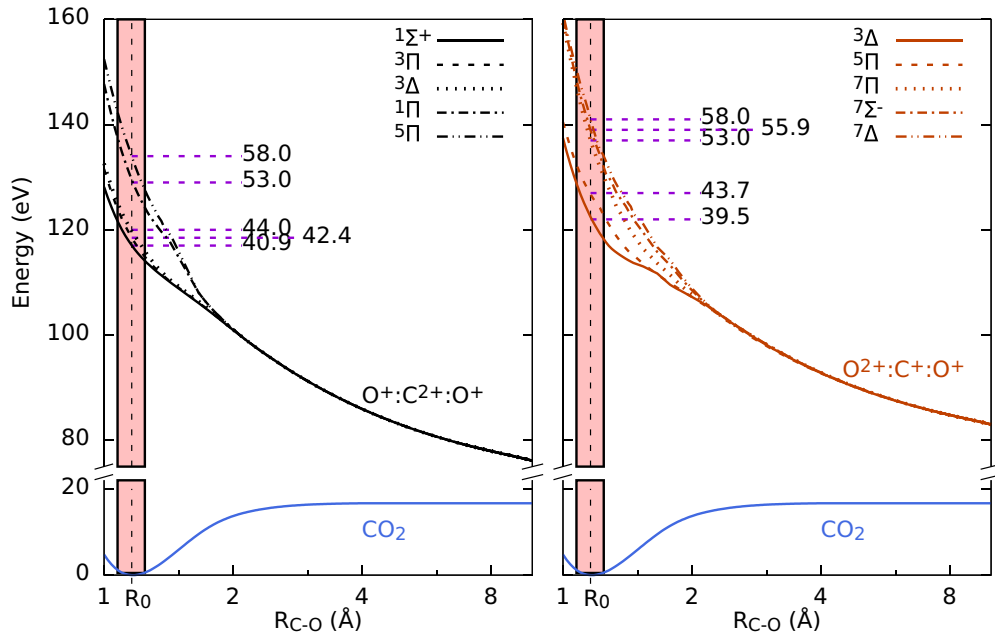


FIG. 1. Potential energy curves of CO<sub>2</sub><sup>4+</sup> calculated using the 6311-G-type basis set. Curves contributing to the (1,2,1) and (2,1,1) fragmentation channels are shown in the left and right panels, respectively. The separated atom limits are O<sup>+</sup>(<sup>4</sup>S), C<sup>2+</sup>(<sup>1</sup>S), O<sup>+</sup>(<sup>4</sup>S), and O<sup>2+</sup>(<sup>3</sup>P), C<sup>+</sup>(<sup>2</sup>P), O<sup>+</sup>(<sup>4</sup>S), respectively. The vertical strip represents the Franck-Condon region. Numbers shown adjacent to the upper curves are the expected values of the kinetic energy release, in eV, resulting from excitation to the respective curves.

### A. Kinetic energy release distributions

The KER distributions of the (1,2,1) and (2,1,1) fragmentation channels under the action of different Ar<sup>q+</sup> ( $8 \leq q \leq 14$ ) ions at same energy of 96 keV are shown in Fig. 2. It is readily noticed that our KER distributions are quite different from the previous results on fragmentation, reported by Siegmann *et al.* using swift HCI [11]. For both channels, they have reported broad KER distributions extending from 25 to 100 eV, with peak values around 57 eV [for channel (1,2,1)] and around 62 eV [for channel (2,1,1)] and lacking a finer structure. They also observed that experimental KER spectra of these two channels are quite similar to each other, which is contrary to our findings. Wang *et al.* have reported some structures in KER distributions of both channels under electron impact [23]. They observed a sharp peak at  $\approx 42.5$  eV with a wide lobe at  $\approx 54$  eV in the (1,2,1) channel and a

weak peak at  $\approx 43$  eV with a lobe at  $\approx 51$  eV in the (2,1,1) channel. However, statistics were very low in these channels because of the low cross section for the formation of CO<sub>2</sub><sup>4+</sup> in electron impact. In our experiment, the KER distribution of the (1,2,1) channel ranges from 30 to 80 eV and that of the (2,1,1) channel ranges from 25 to 90 eV. There are significant differences in the KER distributions of the two channels. The two dominant features in both channels are around 39 eV and around 52 eV. The relative intensities of these two structures are strongly influenced by the projectile charge. For example, for the (1,2,1) channel, the structure around 52 eV is enhanced in the case of Ar<sup>10+</sup> impact (blue curve), while in the case of Ar<sup>12+</sup> impact (black curve), the same feature is suppressed. For the (2,1,1) channel, the Ar<sup>12+</sup> impact (black curve) results in an enhanced relative intensity of the structure appearing around 39 eV in the KER distribution. Apart from these two

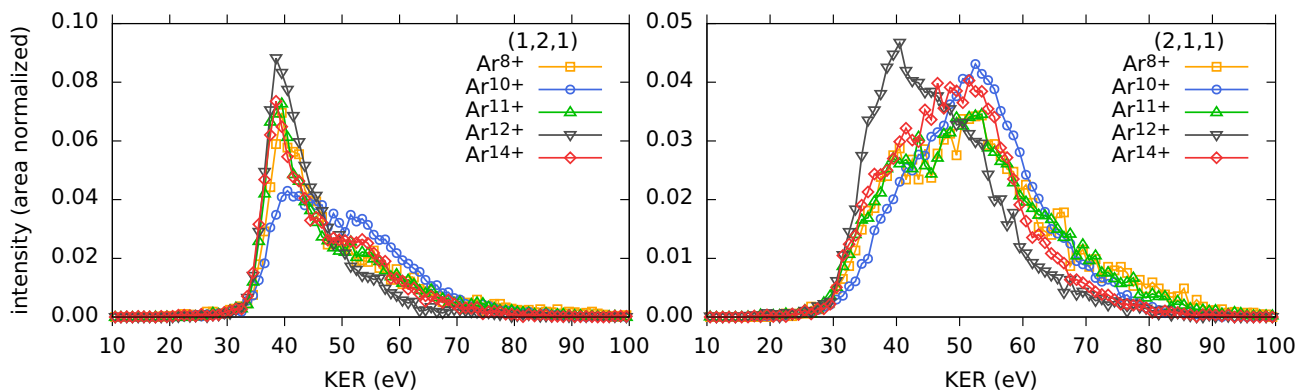


FIG. 2. Total kinetic energy release (KER) distributions resulting from collisions with different Ar<sup>q+</sup> ions at an energy of 96 keV. Left: O<sup>+</sup>:C<sup>2+</sup>:O<sup>+</sup> (1,2,1) fragmentation; right: O<sup>2+</sup>:C<sup>+</sup>:O<sup>+</sup> (2,1,1) fragmentation. Areas under the curves are normalized to unity.

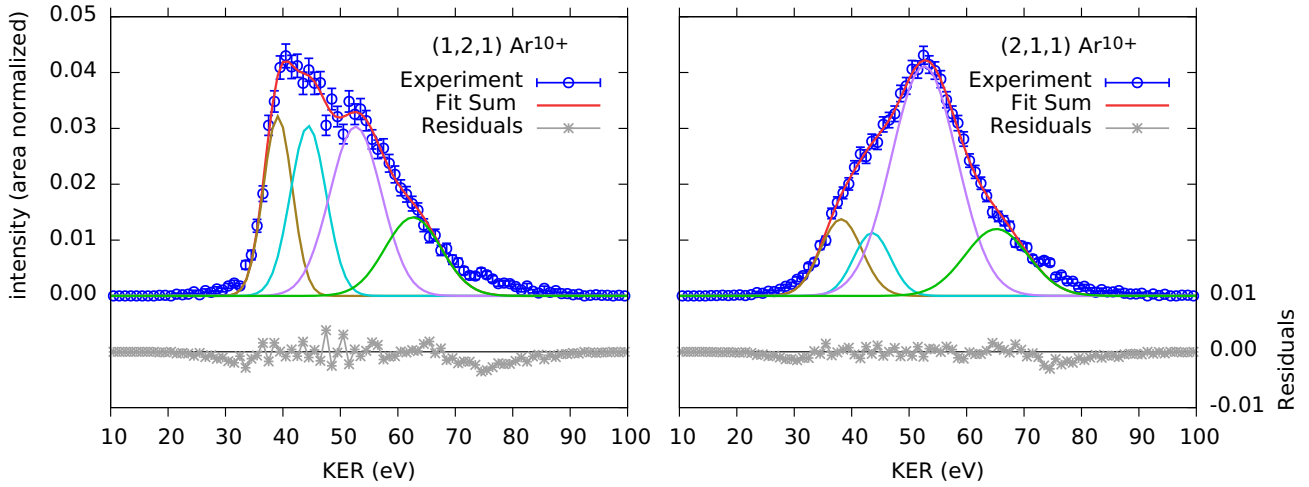


FIG. 3. Fitting of multiple Gaussian curves (normalized to total counts) to experimental KER distributions for  $\text{Ar}^{10+}$  ion impact at 96 keV for the (1,2,1) and (2,1,1) fragmentation channels. Error bars on the experimental data show statistical errors. Fit residuals are shown at the bottom of the graph.

readily observed peaks, there are also some other structures in KER distributions. To identify these, KER distributions of both channels corresponding to different  $\text{Ar}^{q+}$  ions have been fitted to the sum of multiple Gaussian functions.

To obtain the initial parameters for the fit, we take the Franck-Condon region to be  $\pm 2\sigma$  of the probability density of the ground vibrational state of  $\text{CO}_2$  and project this width onto the PEC of upper electronic states (shown in Fig. 1). The projected width is taken to be equal to  $\pm 1.5\sigma$  for the KER distribution. The width of the Gaussian function corresponding to each upper state is fixed in this manner, and is not a fitting parameter, while the amplitudes and centroids of the Gaussians are determined by a least-squares fit of the sum of multiple Gaussians to the experimental KER distributions. Figure 3 shows the experimental KER distribution and the multiple Gaussian fit for both fragmentation channels in the case of  $\text{Ar}^{10+}$  impact. The consistency of the fit has been checked by varying the standard deviation values by  $\pm 10\%$ .

The values of the centroids obtained by fitting are listed in Table I for the two fragmentation channels for all projectiles. These values are compared with the KER values estimated from the PEC for different states, which are also mentioned in the table. A fair agreement is seen between the fitted values of KER and those estimated from the PECs, and this permits us to match the features in the experimental KER distributions with the participating excited states.

We observe, in Table I, that the values of the centroids do not vary much with the projectile charge, except in two instances in channel (1,2,1). For the  $^1\Pi$  excitation, the PEC-based estimate matches the fitted centroids for all projectiles, except  $\text{Ar}^{12+}$ , for which the fitted value is lower. On the other hand, for the  $^5\Pi$  excitation, the PEC-based estimate matches the fitted centroid for  $\text{Ar}^{12+}$ , but the centroids for all other projectiles are higher. As seen from Fig. 2, in the KER distribution beyond approximately 50 eV ( $^1\Pi$  excitation), the tail is longer for projectiles other than  $\text{Ar}^{12+}$ . Since the fit

TABLE I. First two columns: Excited states of  $\text{CO}_2^{4+}$  contributing to the two observed fragmentation channels and the KER values predicted from the computed PE curves and their range based on the Franck-Condon overlap. Next five columns: Centroids (with fitting error) of the Gaussian functions fitted to experimental KER distributions for the two breakup channels for different projectiles. All values are in eV.

Predicted		Centroids of peaks fitted to experimental data				
State and KER		$\text{Ar}^{8+}$	$\text{Ar}^{10+}$	$\text{Ar}^{11+}$	$\text{Ar}^{12+}$	$\text{Ar}^{14+}$
$\text{O}^+ + \text{C}^{2+} + \text{O}^+$ [(1,2,1) channel]						
$^1\Sigma^+$	$40.9 \pm 2.5$	$39.3 \pm 0.1$	$39.1 \pm 0.1$	$38.7 \pm 0.1$	$38.8 \pm 0.1$	$38.4 \pm 0.1$
$^3\Delta$	$44.0 \pm 3.1$	$44.5 \pm 0.4$	$44.4 \pm 0.2$	$44.5 \pm 0.3$	$44.2 \pm 0.4$	$44.3 \pm 0.2$
$^1\Pi$	$53.0 \pm 4.5$	$52.9 \pm 0.8$	$52.7 \pm 0.3$	$53.3 \pm 0.5$	$50.5 \pm 2.2$	$53.0 \pm 0.4$
$^5\Pi$ (or higher)	$58.0 \pm 4.9$	$63.7 \pm 1.5$	$62.7 \pm 0.5$	$64.6 \pm 1.4$	$59.2 \pm 4.5$	$64.7 \pm 1.6$
$\text{O}^{2+} + \text{C}^+ + \text{O}^+$ [(2,1,1) channel]						
$^3\Delta$	$39.5 \pm 3.6$	$38.2 \pm 0.4$	$38.2 \pm 0.4$	$35.3 \pm 0.6$	$36.8 \pm 0.3$	$36.7 \pm 0.2$
$^5\Pi$	$43.7 \pm 3.2$	$44.5 \pm 0.8$	$43.6 \pm 0.4$	$41.2 \pm 0.4$	$41.6 \pm 0.5$	$43.7 \pm 0.3$
$^7\Pi$	$53.0 \pm 5.7$	$52.7 \pm 0.4$	$52.6 \pm 0.1$	$51.5 \pm 0.2$	$49.1 \pm 0.4$	$51.9 \pm 0.2$
higher		$67.2 \pm 0.6$	$65.2 \pm 0.3$	$65.9 \pm 0.4$	$61.8 \pm 1.1$	$65.7 \pm 1.0$

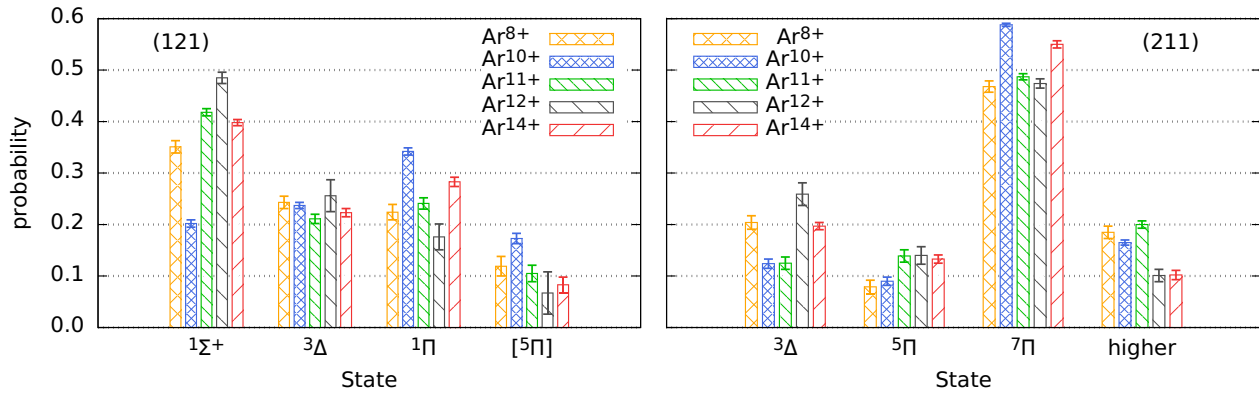


FIG. 4. Probability of excitation to different CO<sub>2</sub><sup>4+</sup> states under the impact of different projectiles, based on the normalized area under each Gaussian function fitted to the experimental KER distribution for the two fragmentation channels, (1,2,1) and (2,1,1). For the (1,2,1) channel, the state shown as [5Π] is to be understood as 5Π, or higher, consistent with Table I.

to the KER distribution is a multippeak fit with peak widths fixed by the Franck-Condon overlap, the dominant structure corresponding to 1Σ<sup>+</sup> and 3Δ excitations causes a shift of the centroids of the neighboring fit functions toward a lower value. For similar reasons, the prominent tail at higher KER for projectiles other than Ar<sup>12+</sup> causes the fitted peaks corresponding to the 5Π excitation for those projectiles to emerge at a higher value.

Referring to Figs. 1 and 2, we see that for channel (1,2,1), the sharp peak around 39.5 eV can be attributed to dissociation of CO<sub>2</sub><sup>4+</sup> via its 1Σ<sup>+</sup> state. The second prominent feature at around 52.5 eV arises by dissociation via the 1Π state, while the features at even higher KER values are due to the dissociation via 5Π or other higher-lying states. For channel (2,1,1), CO<sub>2</sub><sup>4+</sup> dissociates via 3Δ and 7Π states, which give rise to two dominant features in the KER distribution at around 39.5 eV and around 52.0 eV, respectively. Features at higher energy, once again, could be due to higher-lying electronic states, which do not appear in our calculation. Based on the Coulomb explosion (CE) model, the KER value of channel (1,2,1) comes out to be ~56 eV, while for the (2,1,1) channel, it is ~50 eV. However, the experimental value of the average KER for the (1,2,1) channel is lower than that for the (2,1,1) channel for all projectiles—the exact opposite of what the CE model suggests. A similar observation was reported in the work of Siegmann *et al.* [11], and they attributed it to the oversimplification inherent in the CE model, especially in the context of a multielectron system.

The normalized areas of the fitted Gaussian distributions (normalized to the area under the experimental KER distributions for each projectile and each fragmentation channel separately) give us the relative probabilities of the contribution of each state toward the yield of that fragmentation channel. The relative probabilities are shown in Fig. 4. For channel (1,2,1), 1Σ<sup>+</sup>, 3Δ, and 1Π are the main participating electronic states. Of these states, the 3Δ state is almost equally probable for all projectiles. However, the probability of accessing the 1Σ<sup>+</sup>, 1Π, and 5Π states is different for different Ar<sup>q+</sup> ions. The low-lying 1Σ<sup>+</sup> state is dominantly accessed in the case of Ar<sup>12+</sup> impact and the least in the case of Ar<sup>10+</sup> impact. On the other hand, higher-lying states 1Π and 5Π have a

smaller probability in the case of Ar<sup>12+</sup> impact and a greater probability for Ar<sup>10+</sup> impact. Ar<sup>11+</sup> and Ar<sup>14+</sup> show nearly equal probability of accessing the 1Σ<sup>+</sup> state, which is the highest contributing state. For channel (2,1,1), Fig. 4 shows that 3Δ and 7Π are the two main states that are accessed. The 3Δ state is most likely to be accessed in the case of Ar<sup>12+</sup> impact. On the other hand, the 7Π state is more likely to be accessed in the case of Ar<sup>10+</sup>. Furthermore, the dominant 7Π state is almost equally probable for Ar<sup>8+</sup>, Ar<sup>11+</sup>, and Ar<sup>12+</sup> projectiles. Thus, the probability of accessing different electronic states of CO<sub>2</sub><sup>4+</sup> dissociating into (1,2,1) and (2,1,1) channels depends on the projectile charge. Ar<sup>10+</sup> and Ar<sup>12+</sup> are found to show stark differences in the probability of accessing different states, compared to other projectiles, as is also clearly seen in Fig. 2 (blue and black curves). For the (1,2,1) channel, the low-lying 1Σ<sup>+</sup> state has the highest probability of being accessed for all projectiles except Ar<sup>10+</sup>, while the 1Π state has the highest contribution in the case of Ar<sup>10+</sup> impact. For the (2,1,1) channel, the 7Π state has the dominant contribution for all projectiles, and especially so for Ar<sup>10+</sup> impact. For both fragmentation channels, the average KER is lower in the case of Ar<sup>12+</sup> impact compared to all other projectiles.

It should be noted that the (relative) probabilities for higher-lying states are likely to be greater than the estimates based on the observed yields at high KER due to the low collection efficiency for higher-energy fragments, as mentioned in the experimental details. However, this shortcoming will not alter the reported projectile charge dependence for accessing a given excited state.

## B. Correlations between fragment momenta

As discussed in the previous section, the greatest differences in the distribution of the probability of accessing different electronic states of CO<sub>2</sub><sup>4+</sup> are seen for Ar<sup>10+</sup> and Ar<sup>12+</sup> projectiles. In this section, we present the effect of these two projectile ions on fragmentation mechanisms of CO<sub>2</sub><sup>4+</sup> by using a Dalitz plot, which permits visualization of the correlation between fragment ion momenta in terms of the reduced kinetic energy. The *x* and *y* coordinates in a Dalitz

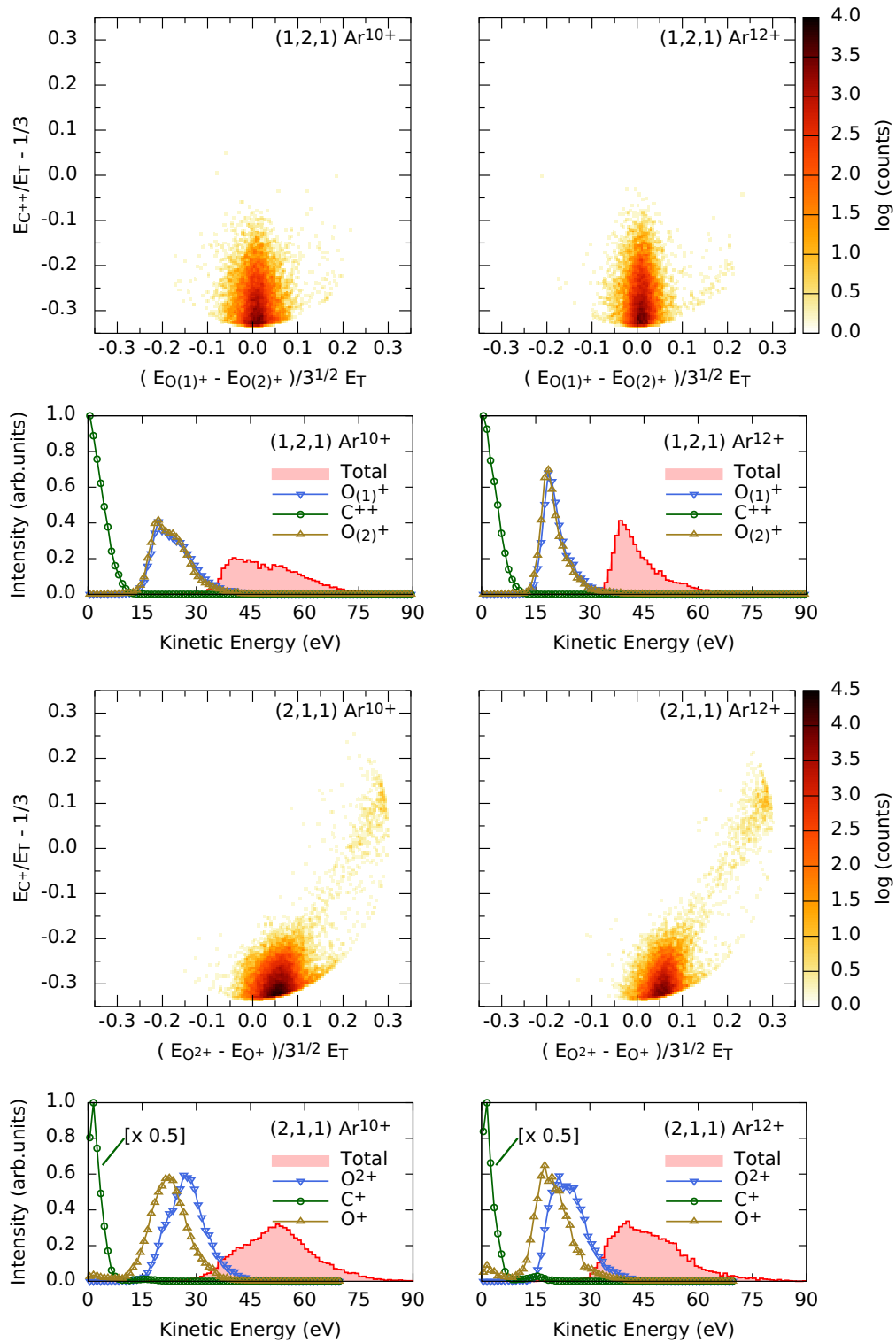


FIG. 5. Dalitz plots and the kinetic energy distributions for the (1,2,1) channel (upper panels) and the (2,1,1) channel (lower panels) for  $\text{Ar}^{10+}$  and  $\text{Ar}^{12+}$  impact. Note that the intensity scale for the KE distribution of  $\text{C}^+$  for channel (2,1,1) has been halved. The counts scale in the Dalitz plots is logarithmic to the natural base.

plot are given by

$$x = \frac{E_1 - E_3}{3^{1/2} E_T}, \quad y = \frac{E_2}{E_T} - \frac{1}{3}, \quad (3)$$

where  $E_i$  ( $i = 1, 2, 3$ ) are the kinetic energies of the three fragments and  $E_T$  is the total kinetic energy release,  $E_T = E_1 + E_2 + E_3$ . For the (1,2,1) channel,  $i \equiv \text{O}_{(1)}^+, \text{C}^{2+}, \text{O}_{(2)}^+$ , and for the (2,1,1) channel,  $i \equiv \text{O}^{2+}, \text{C}^+, \text{O}^+$ .

Dalitz plots for the (1,2,1) channel are shown in Fig. 5 (upper half). The intense region at the bottom ( $x = 0$ ,  $y = -0.33$ ) for both channels reveals that the central ion  $\text{C}^{2+}$  carries very small energy and the two  $\text{O}^+$  ions are emitted back to back, which is a signature  $\text{CO}_2^{4+}$  having a linear geometry. The density distribution in the Dalitz plots is, on the whole, symmetric about the  $x = 0$  axis. This leads to the inference that the (1,2,1) channel is due to a symmetric concerted process. There are no significant differences in the Dalitz plots for the  $\text{Ar}^{10+}$  and  $\text{Ar}^{12+}$  projectiles, except that the spread along the  $x$  axis is greater in the case of  $\text{Ar}^{10+}$  than that for  $\text{Ar}^{12+}$ . The energy sharing among ionic fragments ( $\text{O}^+$ ,  $\text{C}^{2+}$ ,  $\text{O}^+$ ) can be understood directly from the kinetic energy (KE) distributions of each fragment, shown in Fig. 5. It is evident that  $\text{C}^{2+}$  carries away very little energy, and most of the released energy is equally shared by the two  $\text{O}^+$  ions, consistent with a linear, concerted fragmentation. For  $\text{Ar}^{12+}$  impact,  $E_{\text{O}^+}$  distribution has a sharp peak at around 19 eV; however, it has a wider distribution for  $\text{Ar}^{10+}$  impact. This difference is reflected in the spread of Dalitz plots along the direction of the  $x$  axis for both projectile ions.

Dalitz plots for the (2,1,1) channel are shown in Fig. 5 (lower half). In addition to the intense region at the bottom, a weak trace is seen extending towards the top right. The bottom region is asymmetric about the  $x = 0$  axis. It indicates that although the fragmentation leading to the (2,1,1) channel is concerted, it is asymmetric. The  $\text{C}^+-\text{O}^{2+}$  bond stretches more than the  $\text{C}^+-\text{O}^+$  bond. The additional asymmetric weak trace away from the intense region arises due to sequential fragmentation of  $\text{CO}_2^{4+}$  with a final sharing of charges as (2,1,1) via the  $\text{O}^{2+} + \text{CO}^{2+}$  intermediate stage. Khan *et al.* [10] have also observed such weak trace of the sequential fragmentation for this channel. The Dalitz plot for  $\text{Ar}^{10+}$  has a comparatively broader and intense concerted region as compared to  $\text{Ar}^{12+}$ . In the lower panels of Fig. 5, the KE distributions of fragments ( $\text{O}^{2+}$ ,  $\text{C}^+$ ,  $\text{O}^+$ ) show that for the (2,1,1) channel, the peak of carbon ion energy distribution lies slightly above zero because of the asymmetry of the fragmentation. KE distributions of  $\text{O}^+$  and  $\text{O}^{2+}$  ions have peaks at higher values around 22.5 eV and around 27.0 eV for  $\text{Ar}^{10+}$  and lie somewhat lower at around 17.5 eV and around 21.5 eV for  $\text{Ar}^{12+}$ . The small lobe in the KE distributions of  $\text{C}^+$  at around 15 eV and of  $\text{O}^+$  at around 3 eV corresponds to sequential fragmentation, as has been verified by picking up events from regions of the Dalitz plot corresponding to the sequential process. The contribution of the sequential process to total events comes out to be around 6% for  $\text{Ar}^{12+}$  and around 3% for  $\text{Ar}^{10+}$  ion.

## V. CONCLUSION

Three-body fragmentation dynamics of  $\text{CO}_2^{4+}$ , created under the impact of slow HCIs  $\text{Ar}^{q+}$  ( $8 \leq q \leq 14$ ) on  $\text{CO}_2$  at an impact energy of 96 keV, was investigated. Total KER distributions of the fragmentation channels  $\text{O}^+ + \text{C}^{2+} + \text{O}^+$  and  $\text{O}^{2+} + \text{C}^+ + \text{O}^+$  were measured for all  $\text{Ar}^{q+}$  ions. *Ab initio* quantum chemical calculations were carried out to obtain potential energy curves of  $\text{CO}_2^{4+}$  under certain symmetry constraints. With the help of computed PECs, the values of the

KER for both channels were estimated. Experimental KER distributions were fitted to the sum of multiple Gaussian distributions. By comparing the centroids of the Gaussians with the estimated KER values, it was found that the (1,2,1) channel arises mainly via excitation to  $^1\Sigma^+$ ,  $^3\Delta$ , and  $^1\Pi$  states, while the (2,1,1) channel arises mainly via  $^3\Delta$  and  $^7\Pi$  states. The relative probability of accessing these electronic states was found to depend on the charge state of the projectile. For the (1,2,1) channel, the low-lying  $^1\Sigma^+$  was found to have the highest probability of being accessed for all projectiles except  $\text{Ar}^{10+}$ , whereas, for the (2,1,1) channel, the  $^7\Pi$  state was found to dominate irrespective of the projectile, and especially for  $\text{Ar}^{10+}$  impact. Taken together, the most striking difference in the relative contributions of different states was seen between  $\text{Ar}^{10+}$  and  $\text{Ar}^{12+}$  impact, which is likely to be a reflection of different ionization mechanisms being at play for the two projectiles. In fact, for both fragmentation channels, the average KER is found to be the lowest for  $\text{Ar}^{12+}$  impact among all projectiles. Thus,  $\text{Ar}^{12+}$  impact leads to a preponderance of gentler ionization mechanisms than other projectiles; ionization mechanisms leading to higher KER values are suppressed for  $\text{Ar}^{12+}$  impact.

The distribution of the correlated momenta of the fragments, visualized using Dalitz plots, was used to identify concerted and sequential processes. The (1,2,1) fragmentation channel appears entirely via a concerted fragmentation, with symmetric stretching of the two bonds. The (2,1,1) channel is mostly due to concerted fragmentation, with asymmetric stretching of the bonds, accompanied by a small amount of sequential fragmentation, with the doubly charged fragment separating first. The fraction of sequential fragmentation events was found to be higher for  $\text{Ar}^{12+}$  impact than for  $\text{Ar}^{10+}$  impact. For both fragmentation channels,  $\text{Ar}^{10+}$  impact gives a broader momentum distribution compared to  $\text{Ar}^{12+}$  impact.

In summary, low-energy HCIs are seen to be suitable candidates to influence the fragmentation dynamics of polyatomic molecular ions. Depending on the projectile charge, there are differences in the probabilities of participation of different excited states and these lead to patterns in the fragmentation kinematics and dynamics. Different projectiles can lead to a preponderance of certain ionization mechanisms, and this alters the probabilities of populating the excited states that are precursors to fragmentation. Limitations of our experimental setup do not permit separation of the ionization mechanisms, which may be addressed by more involved experimental strategies comprising electron spectroscopy and postcollision projectile charge state analysis. Further insights can be obtained via more accurate and less restrictive calculations of the excited-state potential energy surfaces.

## ACKNOWLEDGMENTS

The authors thank the Science and Engineering Research Board (India) for generous funding which enabled the setting up of the EBIS/A ion source used for this work. They would also like to acknowledge technical help from Dreebit GmbH and assistance from the technical staff at IISER Pune in setting up and running of the machine.

- [1] J. D. Savee, V. A. Mozhayskiy, J. E. Mann, A. I. Krylov, and R. E. Continetti, *Science* **321**, 826 (2008).
- [2] N. Neumann, D. Hant, L. P. H. Schmidt, J. Titze, T. Jahnke, A. Czasch, M. S. Schöffler, K. Kreidi, O. Jagutzki, H. Schmidt-Böcking, and R. Dörner, *Phys. Rev. Lett.* **104**, 103201 (2010).
- [3] Y. Wang, X. Shi, J. Zhou, S. Xu, D. Guo, S. Yan, X. Zhu, and X. Ma, *Phys. Rev. A* **101**, 042706 (2020).
- [4] R. Guillemin, P. Declava, M. Stener, C. Bomme, T. Marin, L. Journel, T. Marchenko, R. K. Kushawaha, K. Jänkälä, N. Trcera, K. P. Bowen, D. W. Lindle, M. N. Piancastelli, and M. Simon, *Nat. Commun.* **6**, 6166 (2015).
- [5] B. Wales, R. Karimi, E. Bisson, S. Beaulieu, M. Giguère, T. Motojima, R. Anderson, J. Matsumoto, J.-C. Kieffer, F. Légaré, H. Shiromaru, and J. Sanderson, *Phys. Scr.* **2013**, 014068 (2013).
- [6] R. Dörner, V. Mergel, O. Jagutzki, L. Spielberger, J. Ullrich, R. Moshhammer, and H. Schmidt-Böcking, *Phys. Rep.* **330**, 95 (2000).
- [7] J. Ullrich, R. Moshhammer, A. Dorn, R. Dörner, L. P. H. Schmidt, and H. Schmidt-Böcking, *Rep. Prog. Phys.* **66**, 1463 (2003).
- [8] A. Khan and D. Misra, *J. Phys. B: At. Mol. Opt. Phys.* **49**, 055201 (2016).
- [9] Z. Shen, E. Wang, M. Gong, X. Shan, and X. Chen, *J. Chem. Phys.* **145**, 234303 (2016).
- [10] A. Khan, L. C. Tribedi, and D. Misra, *Phys. Rev. A* **92**, 030701(R) (2015).
- [11] B. Siegmann, U. Werner, H. O. Lutz, and R. Mann, *J. Phys. B: At. Mol. Opt. Phys.* **35**, 3755 (2002).
- [12] M. R. Jana, P. N. Ghosh, B. Bapat, R. K. Kushawaha, K. Saha, I. A. Prajapati, and C. P. Safvan, *Phys. Rev. A* **84**, 062715 (2011).
- [13] L. Adoui, T. Muranaka, M. Tarisien, S. Legendre, G. Laurent, A. Cassimi, J.-Y. Chesnel, X. Fléhard, F. Frémont, B. Gervais, E. Giglio, and D. Hennecart, *Nucl. Instrum. Methods Phys. Res. Sec. B* **245**, 94 (2006).
- [14] S. Yan, X. L. Zhu, P. Zhang, X. Ma, W. T. Feng, Y. Gao, S. Xu, Q. S. Zhao, S. F. Zhang, D. L. Guo, D. M. Zhao, R. T. Zhang, Z. K. Huang, H. B. Wang, and X. J. Zhang, *Phys. Rev. A* **94**, 032708 (2016).
- [15] E. Wang, X. Shan, Z. Shen, M. Gong, Y. Tang, Y. Pan, K.-C. Lau, and X. Chen, *Phys. Rev. A* **91**, 052711 (2015).
- [16] P. Bhatt, R. Singh, N. Yadav, and R. Shanker, *Phys. Rev. A* **85**, 042707 (2012).
- [17] R. K. Singh, G. S. Lodha, V. Sharma, I. A. Prajapati, K. P. Subramanian, and B. Bapat, *Phys. Rev. A* **74**, 022708 (2006).
- [18] R. K. Kushawaha, S. S. Kumar, I. A. Prajapati, K. P. Subramanian, and B. Bapat, *J. Phys. B: At. Mol. Opt. Phys.* **42**, 105201 (2009).
- [19] W. A. Bryan, J. H. Sanderson, A. El-Zein, W. R. Newell, P. F. Taday, and A. J. Langley, *J. Phys. B: At. Mol. Opt. Phys.* **33**, 745 (2000).
- [20] J. P. Brichta, S. J. Walker, R. Helsten, and J. H. Sanderson, *J. Phys. B: At. Mol. Opt. Phys.* **40**, 117 (2006).
- [21] I. Bocharova, R. Karimi, E. F. Penka, J.-P. Brichta, P. Lassonde, X. Fu, J.-C. Kieffer, A. D. Bandrauk, I. Litvinyuk, J. Sanderson, and F. Légaré, *Phys. Rev. Lett.* **107**, 063201 (2011).
- [22] C. Wu, C. Wu, D. Song, H. Su, Y. Yang, Z. Wu, X. Liu, H. Liu, M. Li, Y. Deng, Y. Liu, L.-Y. Peng, H. Jiang, and Q. Gong, *Phys. Rev. Lett.* **110**, 103601 (2013).
- [23] E. Wang, X. Shan, Z. Shen, X. Li, M. Gong, Y. Tang, and X. Chen, *Phys. Rev. A* **92**, 062713 (2015).
- [24] B. Bapat, D. Sharma, and S. Srivastav, *J. Phys.: Conf. Ser.* **1412**, 152070 (2020).
- [25] M. Schmidt, G. Zschornack, U. Kentsch, and E. Ritter, *Rev. Sci. Instrum.* **85**, 02B704 (2014).
- [26] V. Sharma and B. Bapat, *Eur. Phys. J. D* **37**, 223 (2006).
- [27] W. C. Wiley and I. H. McLaren, *Rev. Sci. Instrum.* **26**, 1150 (1955).
- [28] M. Schmidt, K. Baldrige, J. Boatz, S. Elbert, M. Gordon, J. Jensen, S. Koseki, N. Matsunaga, K. Nguyen, S. Su, T. Windus, M. Dupuis, and J. Montgomery, *J. Comput. Chem.* **14**, 1347 (1993).
- [29] P. G. Szalay, T. Müller, G. Gidofalvi, H. Lischka, and R. Shepard, *Chem. Rev.* **112**, 108 (2012).
- [30] J. H. D. Eland, L. Andric, P. Linusson, L. Hedin, S. Plogmaker, J. Palaudoux, F. Penent, P. Lablanquie, and R. Feifel, *J. Chem. Phys.* **135**, 134309 (2011).
- [31] J. H. D. Eland, M. Hochlaf, P. Linusson, E. Andersson, L. Hedin, and R. Feifel, *J. Chem. Phys.* **132**, 014311 (2010).